

Optimal Dimensioning of Elastic-Link Manipulators regarding Lifetime Estimation

Klaus Zauner^{1*}, Hubert Gatringer¹ and Andreas Müller¹

¹Institute of Robotics, Johannes Kepler University Linz,
Altenbergerstraße 69, Linz, 4040, Austria.

*Corresponding author(s). E-mail(s): klaus.zauner@jku.at;
Contributing authors: hubert.gatringer@jku.at; a.mueller@jku.at;

Abstract

Resourceful operation and design of robots is key for sustainable industrial automation. This will be enabled by lightweight design along with time and energy optimal control of robotic manipulators. Design and control of such systems is intertwined as the control must take into account inherent mechanical compliance while the design must accommodate the dynamic requirements demanded by the control. As basis for such design optimization, a method for estimating the lifetime of elastic link robotic manipulators is presented. This is applied to the geometry optimization of flexible serial manipulators performing pick-and-place operations, where the optimization objective is a combination of overall weight and vibration amplitudes. The lifetime estimation draws from a fatigue analysis combining the rainflow counting algorithm and the method of critical cutting plane. Tresca hypothesis is used to formulate an equivalent stress, and linear damage accumulation is assumed. The final robot geometry is selected from a Pareto front as a tradeoff of lifetime and vibration characteristic. The method is illustrated for a three degrees of freedom articulated robotic manipulator.

Keywords: multibody dynamics, elastic robotic manipulators, multicriterial parameter optimization, fatigue analysis, rainflow method

1 Introduction

Currently, lightweight robots are predominantly used in physical human robot collaboration tasks [1]. However, the need for cost reduction in manufacturing motivates use

of lightweight robots in mass production. Besides lower energy consumption weight reduction of the structure also leads to material savings, but at the expense of increased elastic vibrations. Highly dynamic pick and place trajectories then inevitably lead to vibrations, which have a negative impact on the performance and can also damage the robot. Appropriate trajectory planning and the control are crucial to counteract those effects [2]. Approaches taking into account the inherent flexibility of lightweight robots and of robotic manipulators actuated with compliant drives, e.g. serial elastic and variable stiffness actuators, were developed over the last decade [3–5]. Vibration damping control requires information about the occurring vibrations, however, which are not available in standard industrial robots. In addition to methods that measure the deformation of the robot arms [4], some approaches use measurements from acceleration sensors or inertial measurement units (IMUs) [5]. Depending on the method, these measurements have to be processed in a more or less resource-intensive way and implementation on conventional industrial controllers can be quite challenging.

Novel lightweight robots must be designed and dimensioned strategically [6–11], where CAD modeling and subsequent finite element (FEM) simulation are combined [12]. Instead of computationally expensive FEM simulation and topology optimization, lightweight robots can be constructed from simple geometries, which may later be finetuned. The parameters of the corresponding dynamics model can subsequently be optimized. Every feasible parameter set corresponds to a design candidate. Finding an optimal parameter set under consideration of opposing quality criteria leads to a multi-criterial optimization problem as it often occurs in machine design [13].

A vital part of a lightweight design is to ensure a certain service lifetime based on damage estimation. A viable approach is the conversion of multi-axial stress states to equivalent uniaxial loads by means of a comparative stress hypothesis in order to calculate damage by counting so-called damage events and comparing them with the material characteristics. These are then accumulated according to a damage hypothesis. The service life after which one has to expect cracks in the structure can be estimated from this damage and the duration of the underlying load cycle [14].

The contribution of this paper is a method for fatigue life estimation of robotic manipulators as depicted in Fig. 1, and its use in design optimization. It builds upon preliminary work presented in [15]. The proposed method is a combination of the critical cutting plane method [16, 17] and the linear damage accumulation according to Palmgren and Miner [18]. The rainflow counting algorithm [19–21] is used to identify the load cycles responsible for the damage.

The paper is organized as follows. Modeling and the introduction of the design parameters is carried out in section 2. Section 3 covers the generation of simulation data. The definition and evaluation of design candidates as well as the lifetime estimation is carried out in sections 4 and 5. The methodology, consisting of a parameter study and subsequent fatigue life estimation is illustrated in section 6 using the example of an elastic 3DOF articulated arm robot. Section 7 concludes the paper and gives an outlook on possible future research topics.

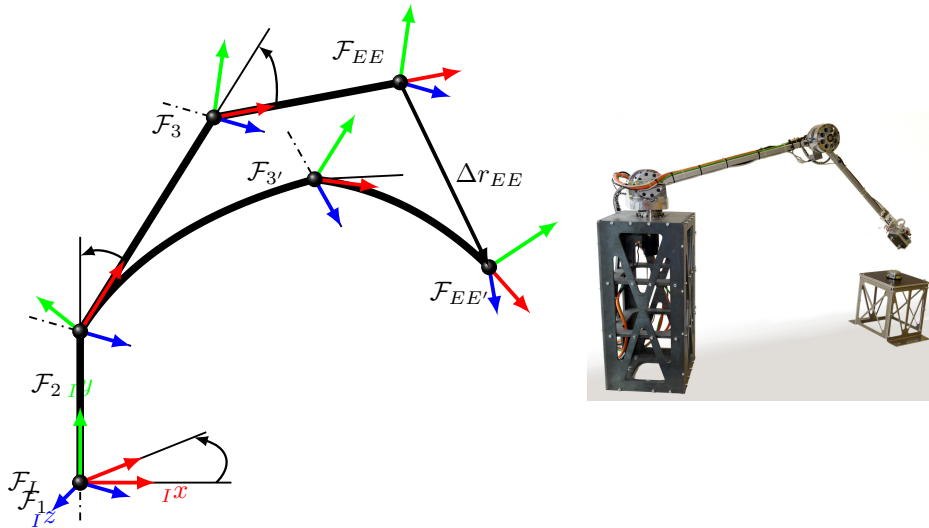


Fig. 1: Elastic manipulator ELLA, Institute of Robotics @ JKU

2 Modeling

The modeling of elastic robots can be carried out in variable detail with regard to the elasticities taken into account. In addition to the gear elasticities and the elasticities of the flexible links, those of joint structures and bearings can also be taken into account. In this paper the focus is on the durability estimation of the elastic links of a serial robot. Detailing on the modeling, especially on the elastic beam modeling for small deformations and the derivation of the equations of motion, can be found in [22] for example.

2.1 Multi-Elastic Links

In general, the links of industrial robots have quite complex geometries. The calculation of their deformations under load therefore usually requires the use of FEM simulations. In the following, the links of a lightweight manipulators are regarded as Euler-Bernoulli beam, which are

- the beam's cross-sections stay normal to the beam's axis,
- the beam's cross-sections stay planar,
- the beam's deflections are small compared to its longitudinal expansion,
- the beam consists of isotropic material and follows Hooke's law.

To derive the equation of motion of the elastic beam, it is divided into infinitesimal slices, hereinafter referred to as elements and each with its own frame \mathcal{F}_E , see Fig. 2. They can be imagined as being threaded along the axis of the beam, which runs through the center of mass (COM) of each of the elements. The beam's longitudinal axis is assigned the coordinate $\xi \in [0, L]$, with L the length of the undeformed beam. The reference frame \mathcal{F}_B of the undeformed configuration is at the origin $\xi = 0$.

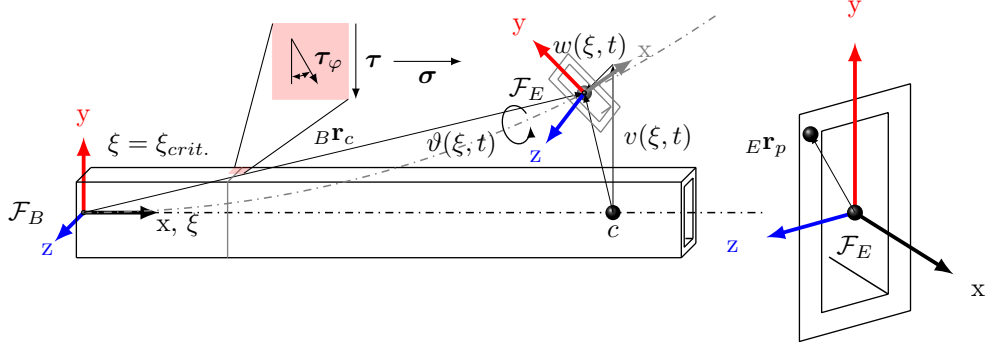


Fig. 2: Elastic link (beam) of an articulated robot, with elastic displacements and critical point for the subsequent lifetime estimation

The COM of an element in the undeformed configuration is denoted as $B \mathbf{r}_c^T = (\xi, 0, 0)$. In the deformed configuration, the vector to the COM and the \mathcal{F}_E frame's orientation are given to

$$B \mathbf{r}_c^T = (\xi \ v(\xi, t) \ w(\xi, t)), \quad B \boldsymbol{\varphi}_c^T = (\vartheta(\xi, t) \ -w'(\xi, t) \ v'(\xi, t)), \quad (1)$$

with $v(\xi, t)$ and $w(\xi, t)$ denoting the time dependent displacement along the y -axis and z -axis respectively. The torsional angle around the x -axis is $\vartheta(\xi, t)$. The normally partial equation of motion of the beam is decoupled with regard to spatial and temporal dependencies, $v(\xi, t) = \mathbf{v}(\xi)^T \mathbf{q}_v(t)$, $w(\xi, t) = \mathbf{w}(\xi)^T \mathbf{q}_w(t)$ and $\vartheta(\xi, t) = \boldsymbol{\vartheta}(\xi)^T \mathbf{q}_\vartheta(t)$, using the direct Ritz-method. Vectors $\mathbf{v}(\xi)$, $\mathbf{w}(\xi)$ and $\boldsymbol{\vartheta}(\xi)$ denote the shape functions. Minimal coordinates $\mathbf{q}_e^T = (\mathbf{q}_v^T \ \mathbf{q}_w^T \ \mathbf{q}_\vartheta^T)$ are the time dependent Ritz coefficients.

The inertia parameters of the differential beam element are given by the differential mass

$$dm_E = \rho A_B d\xi, \quad (2)$$

and the inertia tensor

$$d\mathbf{J}_E = \begin{bmatrix} \rho I_D & 0 & 0 \\ 0 & \rho I_y & 0 \\ 0 & 0 & \rho I_z \end{bmatrix} d\xi, \quad (3)$$

resolved in the element fixed frame \mathcal{F}_E , which is a principal axis system for beams with symmetric cross sections. The cross-sectional area is denoted by A_B , I_y and I_z are the area moments of inertia and I_D is the torsional moment of inertia.

As the beam cross-section remains flat and normal to the beam axis in the deformed state, the position vector of any material point of an element at $\xi = \xi_{\text{crit}}$ ($\xi_{\text{crit}} = 0$ for one side clamped beam) is

$$E \mathbf{r}_p^T = (0 \ y \ z). \quad (4)$$

Linear elastic material behavior

$$\boldsymbol{\sigma} = \mathbf{H} \boldsymbol{\varepsilon} \quad (5)$$

with the Hooke matrix \mathbf{H} and the strain vector $\boldsymbol{\varepsilon}^T = ((-v''y - w''z) \ 0 \ 0 \ -\vartheta'z \ 0 \ \vartheta'y)$ is assumed. Taking into account the assumptions of the Euler-Bernoulli beam, the strain

vector can be rewritten in a reduced form, including only non-zero elements, as

$$\boldsymbol{\varepsilon}_{\text{red}} = \begin{pmatrix} \varepsilon_1 \\ \varepsilon_2 \\ \varepsilon_3 \end{pmatrix} = \begin{bmatrix} 0 & -y & -z \\ -z & 0 & 0 \\ y & 0 & 0 \end{bmatrix} \underbrace{\begin{pmatrix} \vartheta' \\ v'' \\ w'' \end{pmatrix}}_{\boldsymbol{\kappa}} \quad (6)$$

with the curvature $\boldsymbol{\kappa}$. The corresponding, reduced **H**-matrix is

$$\mathbf{H}_{\text{red}} = \begin{bmatrix} E & 0 & 0 \\ 0 & G & 0 \\ 0 & 0 & G \end{bmatrix} \quad (7)$$

with the shear modulus $G = \frac{E}{2(1+\nu)}$, where E is the Young's modulus and ν denotes Poisson's ratio. The beam returns to its undeformed state without an external load. This behavior is modeled by the reaction force $\mathbf{Q}_{el} = -\mathbf{K}_{el}\mathbf{q}_e$ acting on the elastic coordinates, where the stiffness matrix is

$$\mathbf{K}_{el} = \int_0^L \begin{bmatrix} GI_D \boldsymbol{\vartheta}'' \boldsymbol{\vartheta}''^T & 0 & 0 \\ 0 & EI_z \mathbf{v}'' \mathbf{v}''^T & 0 \\ 0 & 0 & EI_y \mathbf{w}'' \mathbf{w}''^T \end{bmatrix} d\xi. \quad (8)$$

It is derived by calculating the deformation related potential energy of the beam. Dynamics modeling according to [22] yields the equation of motion (EOM)

$$\mathbf{M}(\mathbf{q}, \mathbf{p})\ddot{\mathbf{q}} + \mathbf{G}(\mathbf{q}, \dot{\mathbf{q}}, \mathbf{p})\dot{\mathbf{q}} + \mathbf{g}(\mathbf{q}, \mathbf{p}) = \mathbf{Q}_M, \quad (9)$$

with the generalized mass matrix $\mathbf{M}(\mathbf{q}, \mathbf{p})$, the vector of generalized Coriolis and centrifugal forces $\mathbf{G}(\mathbf{q}, \dot{\mathbf{q}}, \mathbf{p})\dot{\mathbf{q}}$, gravitational forces $\mathbf{g}(\mathbf{q}, \mathbf{p})$ and the motor torques \mathbf{Q}_M . The generalized coordinates \mathbf{q} consist of the actuated motor coordinates \mathbf{q}_M , the link sided coordinates \mathbf{q}_L (in case of elastic gearboxes) and the elastic coordinates \mathbf{q}_e . Length-, geometry- and material-parameters are summarized in \mathbf{p} .

3 Load-Case Simulation

The desired model-based design requires data on vibrations and occurring stresses. These must be simulated for a relevant trajectory. A standard application of a lightweight robots are pick and place tasks, ideally with a minimal task duration t_{task} . In general, except when possible collision objects have to be taken into account, only the position ${}_I\mathbf{r}_E$ and the orientation ${}_I\boldsymbol{\varphi}_E$ (e.g. in Cardan-angles) of the end effector, resolved in the inertial frame \mathcal{F}_I , are of particular interest when planning robot motions. The desired time optimization of the movement makes it necessary to consider speed, acceleration and torque limits. Therefore the joint trajectories \mathbf{q}_d need to be computed by the inverse kinematics.

Simulating the robot dynamics at a desired motion \mathbf{q}_d requires solving (9), in combination with an industrial cascaded position controller, for $\dot{\mathbf{q}}$. An efficient $\mathcal{O}(n)$ -algorithm for multibody systems in subsystem representation, as stated in [22], is used to this end. Numerical integration is pursued with an appropriate solver for numerically stiff problems (e.g. `ode15s`).

4 Determination of Candidate Designs

The first step is to identify design candidates that meet the primary quality criteria of weight reduction and low vibration tendency. The structure of the considered manipulator shall be fixed. Therefore its dynamic behavior is determined by EOMs of the form (9) with parameters \mathbf{p} . Every candidate design is basically a set $\mathbf{p}_i \in \mathbf{P}$ out of the set of permissible parameters \mathbf{P} . Vector \mathbf{p} contains several parameters that determine the workspace, which is usually a specification for the robot. Therefore $\mathbf{p} \in \mathbb{R}^{n_p}$ is partitioned into fixed parameters $\mathbf{p}_f \in \mathbb{R}^{n_f}$ and parameters $\mathbf{p}_v \in \mathbb{R}^{n_v}$, which can be adjusted to influence the dynamic behavior of the manipulator.

From the constructive point of view, the parameters that are easiest to change are those of the elastic links. As emphasized in the modeling section 2, these are the material-dependent parameters density and Young's modulus, as well as the geometric parameters cross-sectional area and area moment of inertia. The latter are defined by profile shapes and their dimensions. These can be varied in certain ranges, whereby constructive requirements must also be taken into account. However, these considerations are beyond the scope of this paper and are only carried out for the specific example in section 6.

The aforementioned goals give rise to the multicriterial optimization [13] problem

$$\min_{\mathbf{p} \in \mathbf{P}} (J_m(\mathbf{p}), J_{\text{vib.}}(\mathbf{p}, \mathbf{q}_d(t))) \quad (10)$$

with the $m = 2$ quality criteria $J_m(\mathbf{p})$ which assesses the design dependent robot weight compared to an initial design and $J_{\text{vib.}}(\mathbf{p}, \mathbf{q}_d(t))$ which denotes a quality criteria regarding the endeffector vibration, e.g. the maximum derivation from the desired position during a critical phase of the trajectory.

As these quality criteria are opposing each other, there exists no design that can be clearly identified as the best solution. The so called Pareto front \mathbf{F}_P , see Fig. 8, is defined as the set of candidates that are not outperformed by any other one.

The configurations of the Pareto front are the candidates for the fatigue analysis.

5 Fatigue Analysis

The use of lightweight robots for repetitive tasks to be performed as quickly as possible leads to recurring loads on the bearings of the moving parts (joints, linear guides, ...) and the structural elements (joint structures, arms, ...). Lightweight design is

a decision between the lightest possible constructions and the necessary durability. As this does not allow for large reserves with regard to dynamic loads, it must be estimated during the design process whether the manipulator will achieve the required service life assuming representative load cases. Any correspondingly large load will cause further damage to the structure, so there must be a number of repetitions after which one must at least expect a part of the structure to fail. Let $D \in [0, 1]$ denote a quantification of the damage at an interesting point of the structure during one execution of the representative task. With the task duration t_{task} , an estimate for the lifetime t_{life} (of exactly this part of the structure) is given by

$$t_{\text{life}} = \frac{t_{\text{task}}}{D}. \quad (11)$$

The damage increases over time, therefore an incremental growth ΔD is introduced, which is related to so called damage events.

In the following, the necessary steps for calculating the lifetime estimate are shown.

5.1 Cutting Plane Dependent Stress

Since a beam generally bends and twists under load, this results in a multi-axial stress state with normal and shear components. The stress state at a material point ${}_E\mathbf{r}_p$ (4) is described by the symmetric stress tensor

$$\boldsymbol{\Sigma}_{3D} = \begin{bmatrix} \sigma_{xx} & \sigma_{xy} & \sigma_{xz} \\ \sigma_{xy} & \sigma_{yy} & \sigma_{yz} \\ \sigma_{xz} & \sigma_{yz} & \sigma_{zz} \end{bmatrix} \quad (12)$$

which leads through $\boldsymbol{\sigma}_n = \boldsymbol{\Sigma}\mathbf{n}$ to the stress vector, which depends on the cutting plane with normal vector \mathbf{n} . Since the components under consideration are beams with thin walled cross sections, the simplification to a plane stress state, characterized by $\sigma_{zz} = 0$, $\sigma_{xz} = 0$ and $\sigma_{yz} = 0$, is permissible. Therefore the stress tensor is then

$$\boldsymbol{\Sigma}_{2D} = \begin{bmatrix} \sigma_{xx} & \sigma_{xy} & 0 \\ \sigma_{xy} & \sigma_{yy} & 0 \\ 0 & 0 & 0 \end{bmatrix}. \quad (13)$$

Introducing the cutting frame \mathcal{F}_c , under the cutting angle φ with the axes \mathbf{n} and \mathbf{m} , see Fig. 3, the components of the stress vector are

$$\sigma_{nn} = \frac{\sigma_{xx} + \sigma_{yy}}{2} + \frac{\sigma_{xx} - \sigma_{yy}}{2} \cos(2\varphi) + \sigma_{xy} \sin(2\varphi) \quad (14)$$

and

$$\sigma_{nm} = -\frac{\sigma_{xx} - \sigma_{yy}}{2} \sin(2\varphi) + \sigma_{xy} \cos(2\varphi). \quad (15)$$

Simulation of the elastic beam model from section 2 according to the trajectory and control in section 3 provides the time histories $v(\xi, t)$, $w(\xi, t)$ and $\vartheta(\xi, t)$ of the displacements of the beam axis. The resulting normal and shear stresses are calculated by (5). For every cutting angle φ the shear stress

$$\tau_\varphi(\xi, t) := \sigma_{nm}(\xi, t) = -\frac{1}{2}\sigma_{xx}(\xi, t)\sin(2\varphi) + \sigma_{xy}(\xi, t)\cos(2\varphi) \quad (16)$$

is calculated by (15).

Material characteristics are determined experimentally for uniaxial loading. Therefore, a hypothesis is required to relate the multiaxial stress state to a load-equivalent uniaxial stress state. Tresca's hypothesis is such a relation [23, 24]. According to this hypothesis the equivalent stress is

$$\sigma_{\text{Tresca}} = 2\tau_\varphi(\xi, t), \quad (17)$$

which is assumed to be responsible for the failure of the component. It is mainly used for tough materials under static stress, but is also used for alternating stresses, as it tends to provide a higher equivalent stress and, as a result, greater safety. This hypothesis is used in the subsequent procedure.

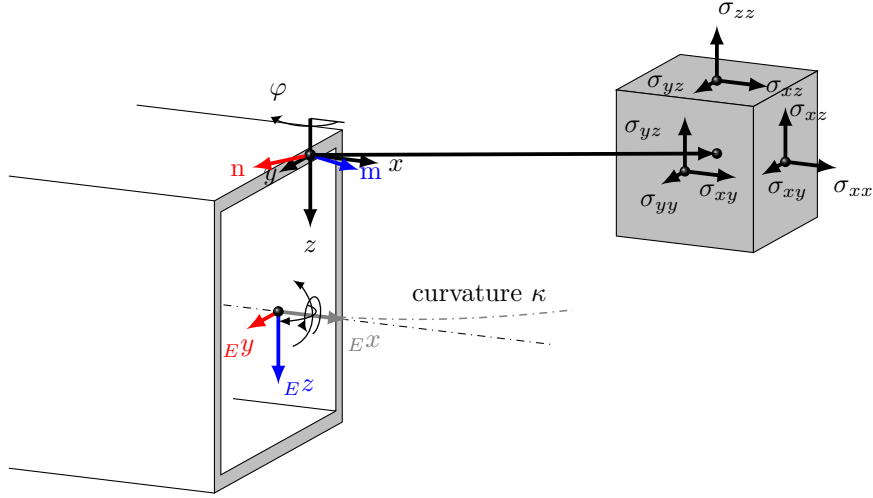


Fig. 3: Stress state in a thin walled beam

5.2 Identifying Damage Events using Rainflow-Counting

As the equivalent stress (17) varies over time the material is loaded and unloaded. A load-cycle with mean stress σ_m and amplitude stress σ_a is generally defined by a

closed loop of the material's uniaxial stress-strain response. Every load cycle, as long as it reaches a certain stress level, see subsection 5.3, further damages the material. In order to be able to accumulate the damage, the damage events must be extracted from the load sequence calculated from (16) by (17). Identifying a load cycle, as depicted in Fig. 4a, is not straightforward for an arbitrary load history Fig. 4b.

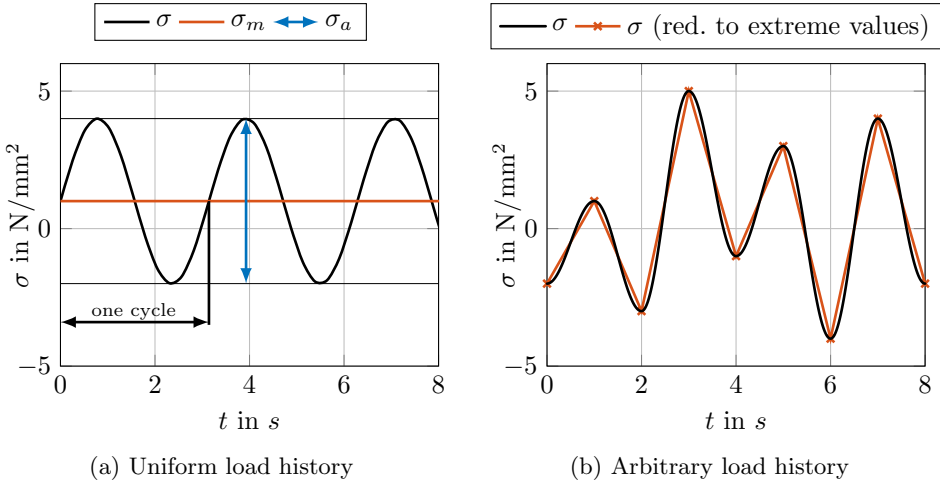


Fig. 4: Definition of mean and amplitude stress (left) and exemplary load history (right)

The rainflow-counting algorithm was developed and proposed by Matsuichi and Endo in 1968 [19]. The continuous time history $\sigma(t)$ of the equivalent stress (17) is reduced to a set of tensile peaks Δ and compressive valleys ∇ , see Fig. 5. The following steps are then carried out:

1. Every tensile peak (Fig. 5 right) / compressive valley (Fig. 5 left) is the source of a flow of water, that would drip down the roofs of a pagoda. Such a flow terminates if one of the following conditions holds:
 - a.) The flow reaches the end of the load duration,
 - b.) it merges with a flow that started before (e.g. Fig. 5 right where green merges into blue),
 - c.) the next tensile peak is of greater or equal magnitude (e.g. Fig. 5 right where orange terminates because blue has a higher starting stress).
2. Each flow, whether tensile or compressive, represents a half cycle with stress magnitude equal to the difference between the stresses at its starting and ending points.

3. One tensile and compressive half cycle each with equal magnitudes are paired up to full cycles. Some half cycles might remain after this step.

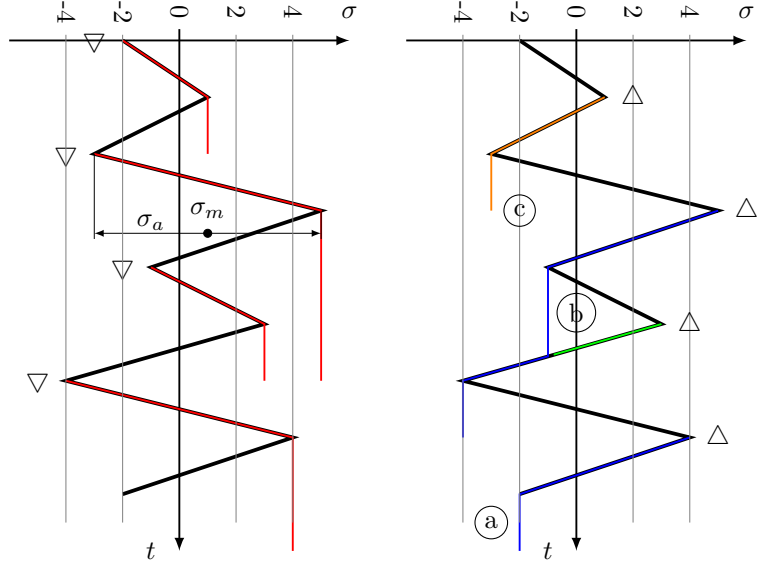


Fig. 5: Pagoda roof method for compressive valleys (left) and tensile peaks (right)

The version of this algorithm, used in the subsequent example, is implemented according to the ASTM E 1049 standard [20].

The mean- and amplitude stresses σ_m and σ_a are naturally continuous quantities. The expected stress ranges are divided into N_m and N_a subranges respectively, which grids the σ_m - σ_a domain under consideration into $N_m N_a$ clusters also referred to as load collectives and referenced by their respective center points (σ_m^*, σ_a^*) . A load collective is a collection of load cycles whose mean and amplitude stresses (σ_m, σ_a) lie within the same cluster (σ_m^*, σ_a^*) . Counting the number $N(\sigma_m^*, \sigma_a^*)$ of occurring events for every cluster results in a histogram, also referred to as rainflow matrix \mathbf{R} .

5.3 Damage Growth ΔD

A damage increase is assigned to each load collective $(\sigma_m^*, \sigma_a^*) \in \mathbf{R}$. This is calculated from the number of cycles $N(\sigma_m^*, \sigma_a^*)$ and the number of fatigue-resistant load cycles in this stress range to

$$\Delta D = \frac{N(\sigma_m^*, \sigma_a^*)}{N(\sigma_{D,a}^*)}. \quad (18)$$

The number of fatigue-resistant load cycles $N(\sigma_{D,a}^*)$ (step 5, see Fig. 6) is extracted from the Wöhler [25] diagram Fig. 6 (right), which is synthetically computed (with

the characteristic point of step 3) according to

$$\frac{\log(R_e) - \log(\sigma_{D,a}^*)}{\log(2 \cdot 10^6) - \log(2 \cdot 10^4)} = \frac{\log(R_e) - \log(\sigma_a^*)}{\log(N(\sigma_a^*)) - \log(2 \cdot 10^4)}, \quad (19)$$

for the specific fatigue-resistant amplitude stress $\sigma_{D,a}^*$ (step 4). This (step 2) in turn is obtained by inserting the load cycle specific mean stress (step 1) into the fatigue strength diagram according to Haigh [26], see Fig. 6 (left). The yield strength is denoted by R_e .

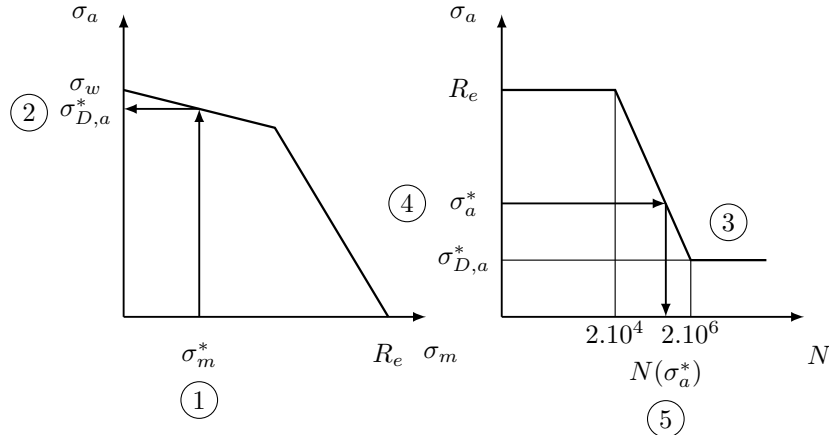


Fig. 6: Haigh-diagram (left) and Wöhler-diagram (right)

5.4 Damage Accumulation

The damage hypothesis is the way in which the total damage is calculated from the damage increments. When calculating those increments in subsection 5.3, the implicit assumption is already made that the chronological order of occurrence of the individual load cycles is irrelevant. Particular materials show hardening effects due to load, which would mean that the sequence of the loads plays a crucial role. In this paper, the linear damage accumulation

$$D = \sum_i \Delta D_i, \quad (20)$$

according to Palmgren and Miner [18] is used, which neglects those effects. The overall damage D is calculated for every cutting angle and the highest damage is used. This approach is referred to as *method of the critical cutting plane* [16].

The methodology is summarized in Alg. 1 and Alg. 2.

Algorithm 1: Lifetime estimation of a critical point in the robot's structure on basis of the *method of the critical cutting plane*.

Input: set of cutting angles Φ
Data: normal and shear stresses $\sigma_{xx}(\xi, t)$ and $\sigma_{xy}(\xi, t)$ at $\xi = \xi_{\text{crit}}$.
for $\varphi \in \Phi$ **do**
 - calculate shear stress (16) and equivalent stress (17);
 - calculate rainflow matrix \mathbf{R} ;
 for \mathbf{R} **do**
 - call Alg. 2;
 - $D(\varphi) := D(\varphi) + \Delta D$ (Palmgren-Miner);
 end
 $D_{\max} := \max(D(\varphi), D_{\max})$ (Critical Cutting Plane)
end
Result: estimated lifetime $t_{\text{life}} := t_{\text{task}}/D_{\max}$

Algorithm 2: Subalgorithm to assign a damage increment to each load spectrum of the rainflow matrix \mathbf{R} .

Input: material specific Haigh diagram
Data: $(\sigma_m^*, \sigma_a^*) \in \mathbf{R}$
begin calculate the related damage growth ΔD
 - fatigue strength $\sigma_{D,a}^*$ for σ_m^* from Haigh diagram;
 - $N(\sigma_a^*)$ from Wöhler line for σ_m^*
end
Result: $\Delta D = N(\sigma_m^*, \sigma_a^*) / N(\sigma_a^*)$ associated to load spectrum

6 Example

The considered articulated robot has three degrees of freedom $\mathbf{q}^T = (q_1 \ q_2 \ q_3)$, see Fig. 7 (right), with gearbox- and link-elasticities. To keep the example clear and concise, only the wall thicknesses of the links are varied. The reference robot's links have a quadratic cross section with edge length $a = 35$ mm and wall thickness $t_i = 4$ mm, $i = 1, 2$. Varying t_1 (first link) and t_2 (second link) between 1 mm and 6 mm leads to 36 possible candidate designs. As only two parameters are varied, the set of configurations \mathbf{C} can be written down as shown in Fig. 7. The reference is configuration 22. The numbering corresponds to that in Fig. 8 and Fig. 9.

6.1 Parameter Study and Determination of Candidate Designs

The intended task for this example is picking an object from a position with corresponding robot configuration \mathbf{q}_{pick} and transporting it to a goal position with $\mathbf{q}_{\text{place}}$. For every q_i , a trajectory with a trapezoidal acceleration profile is planned under consideration of velocity-, acceleration- and jerk-limits.

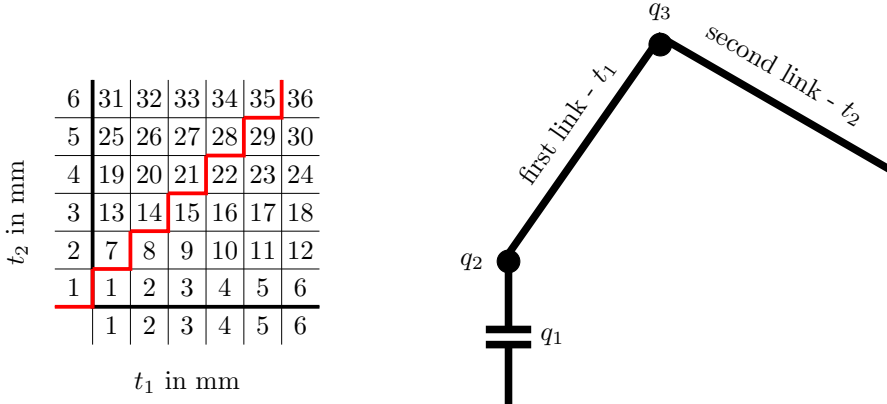


Fig. 7: Configurations for the chosen parameter ranges (left) and scheme of the articulated 3DOF elastic link robot (right)

As can be seen in Fig. 8 the configurations above the red line in Fig. 7 lie within a region of the Pareto diagram which is quite uninteresting, also for the fact, that a second link thicker than the first one, does not make sense. Such configurations could be eliminated beforehand. One can identify groups of six configurations each (e.g. 1 – 7 – 13 – 19 – 25 – 31), which lie on an imaginary curve. Those groups represent configurations with a constant thickness of the first elastic link. They get steeply rising as this thickness decreases and the first part of the kinematic chain is weakened. The weight reduction should be obtained further ahead in the kinematic chain or at least equivalently distributed. As expected, the oscillations of the endeffector increase, as the link stiffness decreases with ongoing mass reduction. With more solid, heavier arms and therefore a stiffer structure, the oscillations nevertheless increase again from a certain point. This is due to the gearbox elasticities, which are excited as the weight of the arms gets higher.

As one is interested in mass reduction, the Pareto front in Fig. 8 defines a set $\hat{\mathbf{C}} = \{1, 2, 3, 4, 5, 6\}$ of interesting configurations, which need to be further investigated.

6.2 Fatigue Analysis of the Candidate Designs

The dynamics simulations of the configurations $\hat{c} \in \hat{\mathbf{C}} \subset \mathbf{C}$ provide with the deformations of the elastic links and therefore the resulting stresses at a specific point. Applying Alg. 1 results in an estimated lifetime for each configuration, see Fig. 9. Some configurations do not reach stresses that go beyond the fatigue strength $\sigma_{D,a}^*$, e. g. $c = 2$. Therefore our specific approach does not yield any damage to the structure which results in an (theoretically) infinite lifetime. The corresponding configurations are marked with an upright triangle. From Fig. 8 and Fig. 9, one can conclude that configurations $\hat{\mathbf{C}} = \{2, 3, 4, 5, 6\}$ are the best with respect to mass reduction, endeffector oscillation and estimated lifetime.

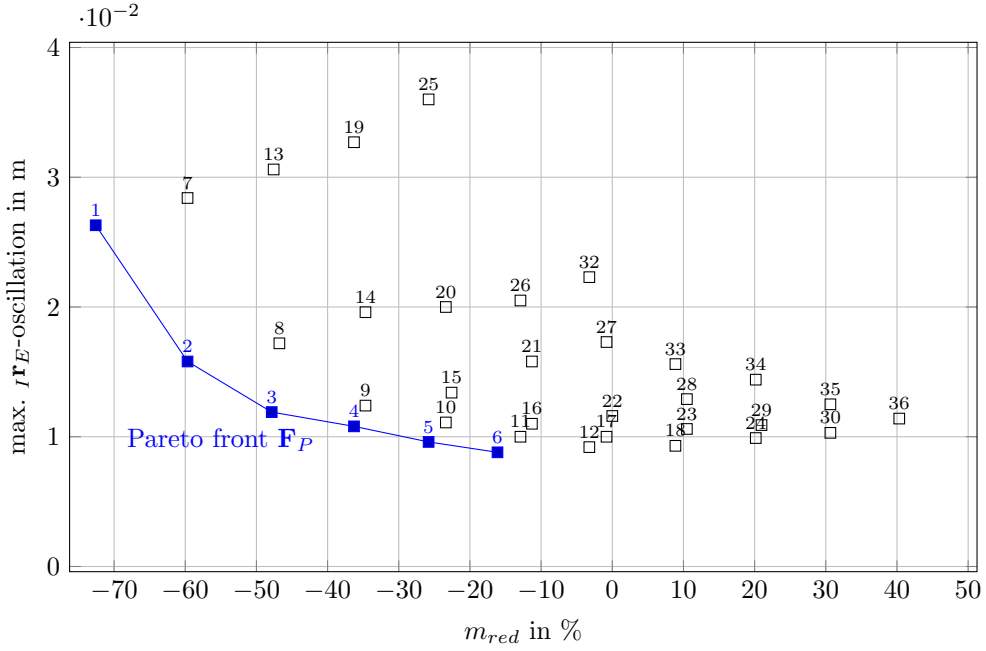


Fig. 8: Pareto diagram: max. $_{IR_E}$ -oscillations via percentage mass reduction m_{red} of the beams compared to the reference configuration

7 Conclusion and Outlook

A optimal design method is presented for optimizing a lumped parameter model of an elastic robot performing pick-and-place operations. The optimality criterion is a combination of the mass of moving links and vibration characteristics. An optimal design can be selected from a Pareto set. To his end, a method for lifetime estimation is presented. The latter combines the rainflow-counting algorithm and the critical cutting plane method using the Tresca equivalent stress hypothesis and assuming linear damage accumulation. The method is demonstrated for an elastic 3DOF robot. The premise of this paper is that elastic deformations are primarily dues to the elastic links and that the link geometries are the only design parameters. It is hypothesized that further weight reduction is possible when elasticities in joints and gears and their mass are taken into account as optimization parameters. The latter becomed more important as the mass of joints and motors becomes more dominant when the links become slender. This will need additional input regarding the equivalent stiffness [27].

Acknowledgments. This work has been supported by the "LCM – K2 Center for Symbiotic Mechatronics" within the framework of the Austrian COMET-K2 program.

References

[1] Bischoff, R., Kurth, J., Schreiber, G., Koeppen, R., Albu-Schäffer, A., Beyer, A.,

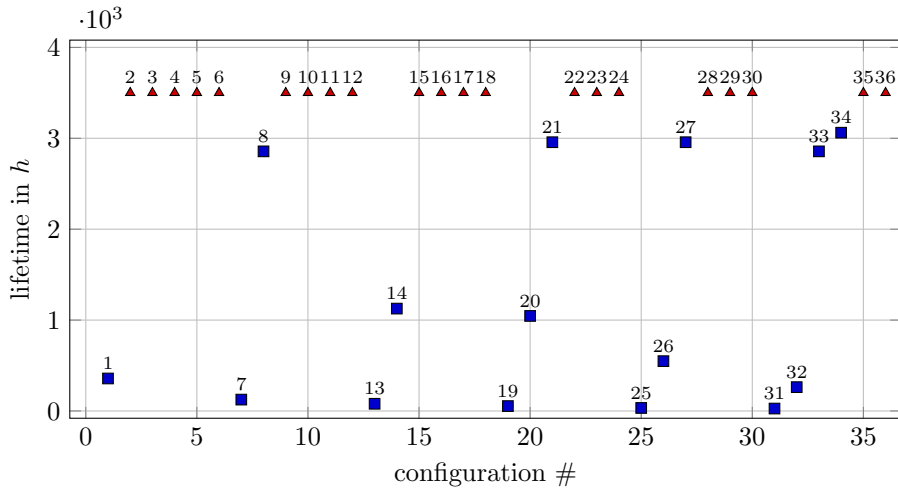


Fig. 9: Estimated lifetime in hours for every $c \in \mathbf{C}$

Eiberger, O., Haddadin, S., Stemmer, A., Grunwald, G., *et al.*: The KUKA-DLR Lightweight Robot arm-a new reference platform for robotics research and manufacturing. In: ISR 2010 (41st International Symposium on Robotics) and ROBOTIK 2010 (6th German Conference on Robotics), pp. 1–8 (2010). VDE

- [2] Springer, K., Gattringer, H., Staufer, P.: On time-optimal trajectory planning for a flexible link robot. In: Journal of Systems and Control Engineering - Proceedings of the Institution of Mechanical Engineers Part I, pp. 752–763 (2013)
- [3] Tsetserukou, D., Kawakami, N., Tachi, S.: Vibration damping control of robot arm intended for service application in human environment. Humanoids 2008 - 8th IEEE-RAS International Conference on Humanoid Robots, 441–446 (2008)
- [4] Malzahn, J.: Modeling and Control of Multi-Elastic-Link Robots under Gravity. PhD thesis, Faculty of Electrical Engineering and Information Technology at TU Dortmund University (2014)
- [5] Staufer, P., Gattringer, H., Bremer, H.: Vibration Suppression for a Flexible Link Robot using Acceleration and/or Angular Rate Measurements and a Flatness Based Trajectory Control. In: Proceedings of the ASME 2011 International Design Engineering Technical Conferences and Computers and Information in Engineering Conference IDETC/CIE (2011)
- [6] Yao, P., Zhou, K., Lin, Y., Tang, Y.: Light-Weight Topological Optimization for Upper Arm of an Industrial Welding Robot. Metals **9**(9) (2019) <https://doi.org/10.3390/met9091020>
- [7] Wang, X., Zhang, D., Zhao, C., Zhang, P., Zhang, Y., Cai, Y.: Optimal design

of lightweight serial robots by integrating topology optimization and parametric system optimization. *Mechanism and Machine Theory* **132**, 48–65 (2019) <https://doi.org/10.1016/j.mechmachtheory.2018.10.015>

[8] Hermle, M., Eberhard, P.: Control and Parameter Optimization of Flexible Robots. *Mechanics of Structures and Machines* **28**(2-3), 137–168 (2000) <https://doi.org/10.1081/SME-100100615>

[9] Panda, S., Mishra, D., Biswal, B.B.: An approach for design optimization of 3R manipulator using Adaptive Cuckoo Search algorithm. *Mechanics Based Design of Structures and Machines* **48**(6), 773–798 (2020) <https://doi.org/10.1080/15397734.2019.1675166>

[10] Alkalla, M.G., Fanni, M.A.: Integrated structure/control design of high-speed flexible robot arms using topology optimization. *Mechanics Based Design of Structures and Machines* **49**(3), 381–402 (2021) <https://doi.org/10.1080/15397734.2019.1688170>

[11] Hussain, F., Mohammadian, M., Goecke, R.: Topology and material optimization of an underactuated robot for gait rehabilitation. *Mechanics Based Design of Structures and Machines* **52**(8), 5308–5325 (2024) <https://doi.org/10.1080/15397734.2023.2252492>

[12] Yin, H., Huang, S., He, M., Li, J.: An overall structure optimization for a light-weight robotic arm. In: 2016 IEEE 11th Conference on Industrial Electronics and Applications (ICIEA), pp. 1765–1770 (2016). <https://doi.org/10.1109/ICIEA.2016.7603872>

[13] Eschenauer, H., Ksoki, J., Osyczka, A.: Multicriteria Design Optimization - Procedures and Applications. Springer, Heidelberg (1990)

[14] Murakami, Y., Miller, K.J.: What is fatigue damage? A view point from the observation of low cycle fatigue process. *International Journal of Fatigue* **27**(8), 991–1005 (2005) <https://doi.org/10.1016/j.ijfatigue.2004.10.009>

[15] Zauner, K., Gatringer, H., Müller, A.: Design Optimization of Multi-Elastic-Link Robots Based on Representative Load Cases. In: Proceedings of the 11th ECCOMAS Thematic Conference on Multibody Dynamics (2023)

[16] Fatemi, A., Shamsaei, N.: Multiaxial fatigue: An overview and some approximation models for life estimation. *International Journal of Fatigue* (2011)

[17] Morel, F., Ranganathan, N., Petit, J., Bignonnet, A.: A Mesoscopic Approach for Fatigue Life Prediction Under Multiaxial Loading. In: Macha, E., Bedkowski, W., Lagoda, T. (eds.) *Multiaxial Fatigue and Fracture*. European Structural Integrity Society, vol. 25, pp. 87–100. Elsevier, Amsterdam (1999). [https://doi.org/10.1016/S1566-1369\(99\)80009-0](https://doi.org/10.1016/S1566-1369(99)80009-0)

- [18] Miner, M.A.: Cumulative damage in fatigue. *Journal of applied mechanics* **12**(3), 159–164 (1945)
- [19] Matsuishi, M., Endo, T.: Fatigue of metals subjected to varying stress. *Japan Society of Mechanical Engineering* (1968)
- [20] Standard Practices for Cycle Counting in Fatigue Analysis. *ASTM E 1049-85* (2017)
- [21] Anthes, R.J.: Modified rainflow counting keeping the load sequence. *International Journal of Fatigue* **19**, 529–535 (1997)
- [22] Bremer, H.: *Elastic Multibody Dynamics - A Direct Ritz Approach*. Springer, Heidelberg (2008)
- [23] Cunha, A., Yanik, Y., Olivieri, C.: Tresca vs. von Mises: Which failure criterion is more conservative in a probabilistic context? *Journal of Applied Mechanics*, 1–8 (2023) <https://doi.org/10.1115/1.4063894>
- [24] Lee, Y.L., Barkey, M.E., Kang, H.T.: *Metal Fatigue Analysis Handbook: Practical Problem-solving Techniques for Computer-aided Engineering*. Elsevier Science, Oxford (2011)
- [25] Murakami, Y., Takagi, T., Wada, K., Matsunaga, H.: Essential structure of S-N curve: Prediction of fatigue life and fatigue limit of defective materials and nature of scatter. *International Journal of Fatigue* **146**, 106–138 (2021) <https://doi.org/10.1016/j.ijfatigue.2020.106138>
- [26] Sendeckyj, G.P.: Constant life diagrams — a historical review. *International Journal of Fatigue* **23**(4), 347–353 (2001) [https://doi.org/10.1016/S0142-1123\(00\)00077-3](https://doi.org/10.1016/S0142-1123(00)00077-3)
- [27] Yin, H., Liu, J., Yang, F.: Hybrid Structure Design of Lightweight Robotic Arms Based on Carbon Fiber Reinforced Plastic and Aluminum Alloy. *IEEE Open Access Journal* **7** (2019)